Biogeosciences Discuss., doi:10.5194/bg-2016-541, 2017
Manuscript under review for journal Biogeosciences
Published: 4 January 2017

Transport and storage of anthropogenic C in the Subpolar North Atlantic : Model – Data comparison

Virginie Racapé[1,2], Patricia Zunino[3], Pascale Lherminier[2], Herlé Mercier[3], Laurent Bopp[1,4], and Marion Gehlen [1]

[1]LSCE/IPSL, Laboratoire des Sciences du Climat et de l'environnement, CEA-CNRS-UVSQ, Orme des Merisiers, Bât. 712, CEA/Saclay, 91190 Gif-sur-Yvette, Cedex, France

[2]IFREMER, Laboratoire d'Océanographie Physique et Spatiale, UMR 6523, CNRS-IFREMER-IRD-UBO, Plouzané, France

[3]CNRS, Laboratoire d'Océanographie Physique et Spatiale, UMR 6523, CNRS-IFREMER-IRD-UBO, Plouzané, France

[4]Département de Géosciences, Ecole Normale Supérieure, 24 rue Lhomond 75005 Paris

Corresponding author : Virginie Racapé, virginie.racape@ifremer.fr

Abstract

The North Atlantic Ocean is a major sink region for anthropogenic carbon (Cant) and a major contributor to its storage. While it is in general agreed that the intensity of the meridional overturning circulation (MOC) modulates uptake, transport and storage of Cant in the North Atlantic Subpolar Ocean, processes controlling their recent variability and 21st century evolution remain uncertain. This study aims to investigate the relationship between the transport of Cant across the Greenland-Portugal OVIDE section and the storage of Cant in the North Atlantic Subpolar Ocean over the past 44 years. Its relies on the combined analysis of a multi-annual data set (OVIDE program) and output from a global biogeochemical ocean general circulation model (NEMO/PISCES) at ½° spatial resolution forced by the atmospheric reanalysis Drakkar Forcing Set 4. The skill of the model to reproduce observed physical and biogeochemical characteristics, as well as their year-to-year variability is assessed over the period covered by observations. While the analysis of the 44 year long hindcast simulation reveals that the interannual variability of the storage rate of Cant is controlled by the northward transport during low NAO phases, as opposed to the air-sea flux during strong NAO phases, the progressive and continuous increase of the subpolar North Atlantic Cant inventory over the period 1958-2012 is driven by the regional uptake of Cant from the atmosphere. Our results suggest thus an increase of the Cant inventory in this region over the 21st century assuming unabated emissions of CO_2 and MOC fluctuation within observed boundaries.

1. Introduction

Since the start of the industrial period and the subsequent rise of atmospheric CO_2, the ocean carbon sink and the inventory of anthropogenic C (Cant) in the ocean have increase substantially (e.g. Sabine et al., 2004; Le Quéré et al., 2009; 2014; Khatiwala et al., 2013). Overall, the ocean has absorbed 28% of all anthropogenic CO_2 emissions, thus providing a negative feedback to global warming and climate change (Ciais et al., 2013). Uptake and storage of Cant are, however, characterized by a significant variability on interannual to decadal time scales (LeQuéré et al., 2015; Wanninkhof et al., 2013) and any global assessment will hide important regional differences, which prevents to detect correctly the change in oceanic sink [Séférian et al., 2014; McKinley et al., 2016).

The North Atlantic Ocean is a key region for Cant uptake (e.g. Sabine et al., 2004; Mikaloff-Fletcher et al., 2006; Gruber et al., 2009) and stores currently as much as 20% of the total oceanic inventory of 155±31 PgC (Khatiwala et al., 2013). Uptake and enhanced storage of Cant in this region result from the combination of two processes: (1) winter deep convection in the Labrador and Irminger Seas, which efficiently transfers Cant from surface waters to the deep ocean (Kortzinger et al. 1999; Sabine et al., 2004; Pérez et al., 2008) and (2) the northward transport of warm and Cant-laden tropical waters by the upper limb of the meridional overturning circulation (MOC; e.g. Àlvarez et al., 2004; Mikaloff-Fletcher., 2006; Gruber et al., 2009; Pérez et al., 2013). Both terms, deep water formation and circulation, are characterized by high temporal variability in response to the leading mode of atmospheric variability in the North Atlantic, the North Atlantic Oscillation (NAO). Hurrell (1995) defined the NAO index as the normalized sea-level pressure difference in winter between Azores and Iceland. A positive (negative) NAO phase is thus characterized by a high (low) pressure gradient between these two systems coupled to strong (weak) westerly winds in the subpolar region. Between the mid-1960s and the mid-1990s, the North Atlantic evolved from a negative to positive NAO phase. The change in wind conditions induced an acceleration of the North Atlantic Current (NAC), as well as increased heat loss and vertical mixing in the subpolar gyre (e.g. Dickson et al., 1996; Curry and McCartney, 2001; Sarafanov, 2009; Delworth and Zeng, 2015). Concomitant enhanced deep convection led to the formation of large volumes of Labrador Sea water (LSW) with a high load of Cant (Lazier et al., 2002; Pickart et al., 2003; Pérez et al., 2008; 2013). Between 1997 and the yearly 2010's, the region undergoes a decline in NAO index. This has caused a reduction of LSW formation (Yashayaev, 2007; Rhein et al., 2011) and a slowing-down of the northward transport of subtropical water by the NAC (Häkkinen and Rhines, 2004; Bryden et al., 2005; Pérez et al., 2013). As a result, the increase in the subpolar Cant inventory is below that expected from rising atmospheric anthropogenic CO_2 levels alone

Biogeosciences Discuss., doi:10.5194/bg-2016-541, 2017
Manuscript under review for journal Biogeosciences
Published: 4 January 2017

(Steinfeldt et al., 2009; Pérez et al., 2013).

Based on the analysis of a time series of physical and biogeochemical properties between 1997 and 2006, Pérez et al. (2013) propose that Cant storage rates in the subpolar gyre are primarily controlled by the MOC intensity. A reduction in the MOC intensity would thus lead to a decrease in Cant storage and would give rise to a positive climate-carbon feedback. The importance of MOC in modulating the North Atlantic Cant inventory was previously suggested by model studies. Those projected a decrease in the North Atlantic Cant inventory over the 21st century in response to a projected MOC slow-down under future climate warming (Crueger et al., 2008). Based on the same sections than Pérez et al. (2013), Zunino et al. (2014) extended the time window of analysis to 1997-2010 and have proposed a novel proxy for Cant transport. It is defined as the difference of the Cant concentration between the upper and the lower limbs of the overturning circulation times MOC intensity (see section C in Supplement for a model-based discussion of the proxy). They observed that while the multi-annual variability of transport of Cant was controlled by the variability of MOC intensity, its long-term change could depend on the increase in Cant concentration in the upper limb of the MOC. As the latter reflects uptake of Cant through air-sea gas exchange at the atmosphere-ocean boundary, it questions the dominant role of ocean dynamics in controlling Cant storage in the subpolar gyre (Pérez et al., 2013). If the storage rate of Cant in the subpolar gyre is indeed at first order controlled by the load of Cant in the upper limb of the MOC, the subpolar Cant inventory is expected to increase along with increasing atmospheric CO_2 - albeit not necessarily at the same rate - and to provide a negative feedback on rising atmospheric CO_2 levels over the 21st century.

The objective of the present study is to evaluate the relationship between Cant transport, air-sea fluxes and storage rate in the Subpolar North Atlantic, along with their combined evolution over the past 44 years (1958-2012). It relies on the combination of a multi-annual data set gathered along the OVIDE section (Mercier et al., 2015) and output from the global biogeochemical ocean general circulation model NEMO/PISCES at 1/2° spatial resolution forced by the atmospheric reanalysis Drakkar Forcing set 4 (DFS4, Bourgeois et al., 2016).

2. Material and methods

2.1. NEMO-PISCES model

This study is based on a global configuration of the ocean model system NEMO (Nucleus For European Modelling of the Ocean) version 3.2 (Madec, 2008). The quasi-isotropic tripolar grid

ORCA (Madec and Imbard, 1996) has a resolution of 0.5° in longitude and 0.5° x cos(ϕ) in latitude (ORCA05) and 46 vertical levels with 10 levels in the upper 100m. It is coupled online to the Louvain-la-Neuve sea ice model version 2 (LIM2) and the biogeochemical model PISCES-v1 (Pelagic interaction Scheme for Carbon and Ecosystem studies; Aumont and Bopp, 2006). Parameter values and numerical options for the physical model follow Barnier et al. (2006) and Timmermann et al. (2005). Two atmospheric reanalysis products, DFS4.2 and DFS4.4, were used for this study. DFS4.2 is based on ERA-40 (Brodeau et al., 2010) and covers the period 1958-2007 while DFS4.4 is based on ERAInterim and covers 2002-2012 (Dee et al., 2011). The simulation was spun up over a full DFS4.2 forcing cycle (50 years) starting from rest and holding atmospheric CO_2 constant to 1870 levels (284 ppm). Temperature and salinity were initialized as in Barnier et al. (2006). Biogeochemical tracers were either initialized from climatologies (nitrate, phosphate, oxygen, dissolved silica from the 2001 World Ocean Atlas, Conkright et al. (2002); preindustrial dissolved inorganic carbon (DIC) and total alkalinity (Alk) from GLODAP, Key et al. (2004)), or from a 3000 year long global NEMO/PISCES simulation at 2° horizontal resolution (Iron and dissolved organic carbon). The remaining biogeochemical tracers were initialized with constant values.

At the end of the spin-up cycle, two 143-year long simulations were started in 1870 and run in parallel. The first one, the historical simulation, was forced with spatially uniform and temporally increasing atmospheric CO_2 concentration (Le Quéré et al., 2014) whereas in the second one, the control simulation, the mole fraction of CO_2 was kept constant in time at 1870 level. Both runs were forced by repeating 1.75 cycles of DFS4.2 interannually varying forcing over 1870 to 1957. Then DFS4.2 was used from 1958 to 2007. Simulations were extended from 2002 to 2012 by switching to DFS4.4. No significant differences were found in tracer distributions and Cant related quantities between both atmospheric forcing products during the years of overlap (2002-2007). Carbonate chemistry and air-sea CO_2 exchanges were computed by PISCES following the Ocean Carbon Cycle Model Intercomparison Project protocols (www.ipsl.jussieu.fr/OCMIP) and the gas transfer velocity relation provided by Wanninkhof (1992). Cant concentrations and anthropogenic CO_2 fluxes were calculated as the difference between historical (total C) minus control (natural C component) simulations. The global ocean inventory of Cant simulated by the model in 2010 amounted to 126 PgC. It is at the lower end of the uncertainty range of the estimate by Khatiwala et al. (2013) of 155±31 PgC (Fig. 1). At the global scale, the error of the model is close to 6% (values excluding arctic regions and margin seas). The mismatch between the modeled Cant inventory and that of Khatiwala et al. (2013) is largely explained by the difference in the starting year of integration: 1870 for this study as opposed to 1765 in Khatiwala et al. (2013). The coupled model configuration is referred to as ORCA05-PISCES hereafter. The reader is invited to refer to Bourgeois et al. (2016) for a detailed description of model and simulation strategy.

This study followed a two-step approach. The model was first evaluated against the OVIDE data set from year 2002 to 2010 (DFS4.4). The data set consists of observations for June only (see below). As the water column distribution of hydrological and biogeochemical properties are comparable between May and July, model output was subsampled along the section in June for a comparison to data (Tables 1 and 2). Next, the period of study is extended to 1958-2012 (DFS4.4 up to 2001; DFS4.4 over 2002 to 2012) to study the long-term variability of the Cant fluxes, storage and budget.

2.2. OVIDE data set

Observations used to evaluate model output from ORCA05-PISCES in the North Atlantic Ocean were collected within the framework of the OVIDE program. The program aims to document and understand the origin of the interannual to decadal variability in circulation and properties of water masses in the Subpolar North Atlantic in the context of climate change (http://www.umr-lops.fr/Projets/Projets-actifs/OVIDE). Since 2002, one spring-summer cruise is run every two years (Table 1) between Greenland and Portugal following the track presented on figure 2. Dynamical (ADCP), physical (Temperature -T- and Salinity -S-) and biogeochemical (e.g. Alk, pH, dissolved oxygen -O_2- and nutrients) properties are sampled during each cruise at full depth hydrographic stations spaced by 25 nautical miles (NM) and reduced to 16 NM in the Irminger sea and 12 NM or less over steep topographic features. An overview of instruments, analytical methods and accuracies of each parameter is summarized in Zunino et al. (2014). pH and Alk are used to calculate the concentration of DIC following the recommendations and guidelines from Velo et al. (2010). DIC is used in turn together with T, S, nutrients, O_2 and Alk to derive the Cant concentration following the φCT method (Pérez et al., 2008; Vàzquez-Rodrìguez, 2009). This data-based diagnostic approach uses water mass properties of the subsurface layer between 100-200m as reference to evaluate preformed and disequilibrium conditions. The random propagation of errors associated with input parameters yields an uncertainty of 5.2 µmol kg^{-1} on C_T values (Pérez et al., 2010). The OVIDE data set is available for the period 2002-2010 on the CARINA website (http://cdiac.ornl.gov/oceans/CARINA/; Table 1).

2.3. Diagnostic of Cant transport and budget

Transport of Cant across a section

The simulated transport of Cant (T_{Cant}) across a section is evaluated either from online or from offline diagnostic for each ORCA05 grid-level. The transport of Cant is then integrated vertically from bottom to surface and horizontally from the beginning (A) to the end (B) of a section along a continuous line defined by zonal (y) or meridional (x) grid segment (Fig. S1). Positive values stand for northward and/or eastward transport (see section A in Supplement for the description of section).

In the online approach, the transport of Cant (${}^{m}T_{Cant}{}^{online}$) is the sum of the advection (${}^{m}T_{Cant}{}^{adv}$), the diffusion (${}^{m}T_{Cant}{}^{lf}$) and the eddy (${}^{m}T_{Cant}{}^{eiv}$) contribution (Eq. (1)). The ${}^{m}T_{Cant}{}^{adv}$ term corresponds to the product of velocities orthogonal to the section (V) times Cant concentration ($[Cant]$). The ${}^{m}T_{Cant}{}^{lf}$ term is the transport of Cant due to the horizontal diffusion. Finally, the ${}^{m}T_{Cant}{}^{eiv}$ term is the transport of Cant due to eddies; it is based on the use of Gent and McWilliams (1990) parameterization. All these terms are diagnosed online and averaged over 5-days for the period 2003-2011.

$${}^{m}T_{Cant}^{online} = \left[{}^{m}T_{Cant}^{adv} + {}^{m}T_{Cant}^{lf} + {}^{m}T_{Cant}^{eiv}\right]^{online} \qquad (1)$$

In the offline approach, Cant transport is reduced to the advective component because the contribution of diffusion and eddies are negligible for sections studied in the model (see Fig. S2) that echoes results from Treguier et al. (2006) for the OVIDE section. Evaluation of the advective transport of Cant is based on 1) monthly averaged model output over the period 2002-2010 to compare to observation-based results along the OVIDE section (Zunino et al., 2014), and 2) yearly averaged model output over the period 1958-2012 to study the long-term variability of Cant fluxes and storage rates. This last evaluation is completed by the heat transport. It is evaluated in ORCA05-PISCES simulations from velocities orthogonal to the section (V) and the heat term provided by the international thermodynamic equations of seawater (TEOS 2010).

Budget of Cant in the North Atlantic Ocean

The budget of Cant is computed for three North Atlantic regions (see below for definition of regions). This budget is defined as the balance between i) the time rate of change in Cant, vertically and horizontally integrated, ii) the incoming and outgoing transport of Cant across boundaries of each region and iii) the anthropogenic air-sea CO_2 exchange, spatially integrated. This is then completed by the heat transport for the period 2003-2011. All terms are estimated from model output either from monthly or yearly averages depending on the period analyzed (monthly for 2003-2011; yearly for 1958-2012). Finally, relationships between Cant fluxes and its storage rate are investigated for each region. A moving average (windows:12 month for 2003-2011, 10 years for 1958-2012) has been used beforehand for the smoothing of times series data, followed by a leastsquare fit to remove linear trend. Results of smoothing are displayed on Fig. S3.

3. Model evaluation over the OVIDE period

3.1. Distribution of hydrological and biogeochemical parameters along the Greenland-Portugal OVIDE section

Figure 3 illustrates the distribution of salinity (a and b), dissolved oxygen (c and d) and dissolved silica (e and f) concentrations along the Greenland-Portugal OVIDE section, as simulated by ORCA05-PISCES (a, c and e) and compared to the OVIDE data set (b, d and f). The distributions of these hydrological and biogeochemical tracers are characterized by typical regional features which reflect the origin and properties of water masses. These regional features are particularly useful for the validation of model simulations.
The highest salinity along the section is found in surface and subsurface waters of the Eastern North Atlantic and Iberian basin (east of 1500 km, Fig. 3b). It corresponds respectively to East North Atlantic Central Water (ENACW) and to Mediterranean Water (MW) (Harvey, 1982; Tsuchiya et al., 1992; Pollard et al., 1996, van Aken and Becker, 1996, Àlvarez et al., 2004). While these properties are well reproduced by the model (Fig. 3a), simulated salinity maxima are either underestimated for MW (S^{ORCA05}>35.6 vs S^{OVIDE}>36.1, García-Ibáñez et al., 2015; Fig. 3a) or lack the expected distribution for ENACW (values too high or too small compared to observations). There is another core of relatively high salinity in both the OVIDE data (Fig. 3b) and the model output (Fig. 3a). It is located in the subsurface water over the Reykjanes Ridge and reflects the influence in the subpolar region of the saltier central Atlantic water carried by the Eastern Reykjanes Ridge Current (ERRC) derived from the NAC (Pickart et al., 2005; Våge et al., 2011; Daniault et al., 2016).

In the water column, two cores of relatively low salinity and high O_2 concentration are identifiable on both sides of the Reykjanes Ridge in the OVIDE data (Fig. 3d). They are reproduced by ORCA05-PISCES (Fig 3c), albeit with lower levels than the in-situ data ($O_2^{ORCA05} > 260$ µmol kg^{-1} vs $O_2^{OVIDE} = 285 \pm 2$ µmol kg^{-1}, García-Ibáñez et al., 2015). They are consistent with the two pathways of LSW (Pickart et al., 2003; Alvarez et al., 2004; Daniault et al., 2016) and take up the largest volume of water of the section like in García-Ibáñez et al. (2015).

High dissolved silica ($Si(OH)_4$) concentrations below 2500m depth in the Iberian basin (Fig. 3f) correspond to the lower limb of North-East Atlantic Deep Water (NEADWl), which is predominantly formed by the mixing between the recirculation of Iceland-Scotland Overflow Water

(ISOW), rich in oxygen, and the Antarctic Bottom Water (AABW), poor in oxygen but rich in $Si(OH)_4$ (van Aken and Beker, 1996; van Aken et al., 2000, García-Ibáñez et al., 2015). In the model, the $Si(OH)_4$ signal characteristic of NEADWl is identified in the same location, but it is stronger and associated to a lower oxygen concentration compared to OVIDE ($Si(OH)_4^{ORCA05} > 55$ µmol kg^{-1} vs $Si(OH)_4^{OVIDE} < 50$ µmol kg^{-1}, Figs. 3e and f; $O_2^{ORCA05} < 200$ µmol kg^{-1} vs $O_2^{OVIDE} >$ 230 µmol kg^{-1}, Figs. 3b and c). Moreover, high values of simulated dissolved silica concentrations are found in the deep Iceland and Irminger basins, contrasting with observations. Both basins are generally occupied at depth by Denmark Strait Overflow Water (DSOW) and by ISOW. Recently ventilated in the Artic region (Rhein et al., 2002; Tanhua et al., 2005), DSOW and ISOW result from a complex mixture of various water masses and flow over the bottom along the Greenland continental slope and on both sides of the Reykjanes Ridge (Tanhua et al., 2005; Yashayaev et Dickson, 2008; García-Ibáñez et al., 2015). The DSOW is traced by its maximum in O_2 (>280 µmol kg^{-1}, Rhein et al., 2002; García-Ibáñez et al., 2015) and its relative minimum in nutrients (< 15 µmol kg^{-1}, Fig. 3c; Tanhua et al., 2005), whereas the ISOW is characterized by a relative maximum in salinity (close to 35, García-Ibáñez et al., 2015). The comparison between observed (Figs. 3b, d and f) and simulated (Figs. 3a, c and e) properties suggests that the model fails to correctly reproduce dense overflows. The underestimation of DSOW and ISOW by the model results in a predominant contribution of water masses coming from the Antarctic to deep waters in the Iceland and Irminger basins.

3.2. Mass transport across the Greenland-Portugal OVIDE section

Figure 4 illustrates the monthly evolution of the net volume transport across the Greenland-Portugal OVIDE section from model simulations over the period 2002-2010. Values vary between -0.46 Sv ($1 \text{ Sv} = 10^6 \text{ m}^3\text{s}^{-1}$) and 1.88 Sv without any clear and obvious seasonal cycle. As expected, the net transport is towards the North (Lherminier et al., 2007; Mercier et al., 2015) with a mean annual flow of 0.67 ± 0.46 Sv. Compared to estimates derived from the OVIDE data set for the month of June, the model simulates a net transport in line with these estimates for June 2002 and 2004, but underestimates the net transport by up to 50% for June 2006 and 2008, respectively and by up to 120% for June 2010 (Table 2). Considering the large modeled month-to-month variability of net transport, the model misfit could correspond to a slight phase shift between modeled and true yet unresolved variability. If indeed the net transport is as variable as suggested by ORCA05-PISCES on sub-seasonal to interannual time scales, then observation-based estimates derived for June only would not represent the annual mean value. This is confirmed for the model by an independent two samples t-test, which rejects the null hypothesis of the averaged-mass transport computed for the month of June (0.19 ± 0.33 Sv; Table 2) being representative of the annual mean.

The computation of mass transport using a meridional overturning stream function (see section C in Supplement for details) reveals a vertical and horizontal accumulated arrangement in ORCA05-PISCES in relative agreement with the OVIDE data set (Fig. 5). The model does, however, not reproduce the interannual variability present in observations (Figs. 5a and 5b). Moreover, it underestimates the magnitude of MOC by around 2 Sv (with a model estimate at 13.4±0.6 Sv vs 15.5±2.3 for OVIDE-based estimate, Mercier et al., 2015; Table 2). The upper limb of the MOC, the NAC (Lherminier et al., 2010), flows northeastward in the Eastern part of the section (East of 1100 km; Fig. 5b), with its modified branch, the Irminger Current, in the Western part (around 700km off the Greenland Coast) in model and data as defined by Mercier et al. (2015) (Fig. 5b). The NAC is simulated with a lower variability and weaker intensity (Fig. 5b; ORCA05-PISCES increase in cumulative mass transport of 15 Sv instead of 25 Sv between 1100km and 2500km from Greenland coast). In addition, the vertical stream function (Fig. 5a) reveals a stronger current between the surface and the density anomaly (σ_1) 31.5 kg m^{-3} in the model, only observed at the east of the Reykjanes Ridge (not show here). This overestimation of the overturning stream function in the model is likely due to a shift in the position of the Western limit of the NAC. The Western limit is detected close to zero values for mass transport. It occurs around 1000 km off Greenland in the model, instead of 1300 km in observations (Fig. 5b).

The lower limb of MOC, mainly related to the Western Boundary Current (WBC), flows southward in the western part of the section (Lherminier et al., 2007; 2010; Mercier et al., 2015). Sigma 1 separating both limbs of the MOC simulated by the model is lower (32.01±0.01 kg m^{-3}) than those estimated with in situ data (32.14 kg m^{-3}). It follows that the lower (upper) limb in the model takes up a bigger (smaller) volume along the section in the model compared to the OVIDE data set (Fig. 6). The model underestimates the intensity of the southward transport of the WBC in the Irminger Sea, and the ERRC in the Iceland basin (Fig. 5b), which are the most intense currents flowing in the lower limb of the MOC. It also underestimates the cumulative mass transport for σ_1 >32.40 kg m^{-3} (σ_0 >27.7 kg m^{-3}), which is close to 0 Sv in the model (Fig. 5a) as opposed to 7 Sv recorded by Lherminier et al. (2007) and García-Ibáñez et al. (2015). These densest water masses correspond to NEADWl, DSOW and ISOW. Taken together, the misfit between observation-derived estimates and modeled mass transport being the largest in the Irminger and Iceland basins and the preceding discussion of biogeochemical properties (III.1) suggest that the significant underestimation of mass transport in the highest density classes is probably due to the close to zero contribution of overflow waters to the transport in the model at the latitude of the OVIDE section.

Finally, mean values of the magnitude of the MOC computed for the month of June from model output over the period 2002-2010 are equal to the annual average computed over the same period (two sampled t-test; 13.4 ± 2.4 Sv, Table 2). However, its variability computed as the standard deviation of June estimates (± 0.6 Sv) is not representative for its variability in ORCA05-PISCES when computed over the full period (± 2.4 Sv, Table 2).

3.3. Cant distribution along the Greenland-Portugal OVIDE section

Concentrations of Cant computed by the model or from the OVIDE data set represent estimates derived by two inherently different approaches: the former is the difference between two simulations (historical minus control), the latter is computed following the φCT method (sections II.1 and II.2). Both methods yield comparable distributions along the OVIDE section with higher concentrations in surface waters and lower levels at depth (Figs. 6a and 6b). The surface to depth gradient is more pronounced in the Eastern basin. The two LSW cores, relatively rich in Cant, are present on both sides of the Reykjanes Ridge. During the OVIDE period, values simulated by ORCA05-PISCES are nevertheless lower by 6.3±0.6 µmol kg^{-1} compared to observed-based estimates (Table 2). This deficit is more pronounced in the upper limb of MOC (ΔCant$^{\text{model-data}}$ = -5.9±0.7 µmol kg^{-1}) than in the lower limb (ΔCant$^{\text{model-data}}$ = -3.6±0.6, Table 2). The largest difference between model and data, up to -20 µmol kg^{-1} (Fig. 6c), is detected in the subsurface waters at the transition between ENACW and MW and between both limbs of the MOC. Its interannual variability (standard deviation (of model-data) up to 10 µmol kg^{-1}; Fig. 6d) is also largest at the boundary between upper and lower limbs of the MOC, mainly between 700 km to 2000 km off Greenland. The higher interannual variability in this region could be explained by the interannual variability of the NAC intensity, which is underestimated by ORCA05-PISCES. Moreover, this region is also a potential area for mode water formation (de Boisséson et al., 2012), but this processus has not been studied in this paper. It is not the scope of this paper. Figure 6 also reveals an underestimation by the model of Cant levels in NEADWl by 5 to 10 µmol kg^{-1} which is in line with a close to zero contribution of dense Cant rich overflow waters along the OVIDE section.

3.4. Budget of Cant in the North Atlantic Ocean (north of 25° N)

Figure 7 summarizes the budget of Cant in the North Atlantic simulated by the model over the period 2003-2011. In order to facilitate the comparison of the modeled budget to Pérez et al. (2013), we defined two boxes separated by the Greenland-Portugal OVIDE section. The first one extends from 25° N to the OVIDE section; the second box extend from the OVIDE section to the Nordic sills. Seasonality was removed beforehand using a 12-month running filter (section II.3).

In the model, over one third of Cant entering in the southern box at 25° N (0.092±0.016 PgC yr^{-1}) is transported across the OVIDE section (0.035±0.005 PgC yr^{-1}) and leaves the domain at the Nordic sills (0.034±0.004 PgC yr^{-1}). The latter corresponds to a net northward transport resulting from a northwards flux across the Iceland-Scotland strait (0.053±0.005 PgC yr^{-1}) and a southward flux across the Denmark strait (-0.020±0.014 PgC yr^{-1}). The remainder of the regional Cant storage is provided by the air to sea exchange with the largest values south of the OVIDE section (South: 0.156±0.008 PgC yr^{-1}; North 0.044±0.003 PgC yr^{-1}). As a consequence, 88% of the incoming Cant flux (computed as (0.092 + 0.156+0.044-0.034)/(0.092 + 0.156+0.044); Fig. 7) is stored inside the region every year, predominantly south of the OVIDE section (South : 0.216±0.019 PgC yr^{-1} ; North : 0.045±0.006 PgC yr^{-1}).
Compared to the previous studies of Pérez et al. (2013) and Zunino et al. (2014; 2015a and b), the transport of Cant is three time smaller at 25° N and the OVIDE section and two time smaller at the sills. From our discussion in sections III.2 and III.3, it follows that the underestimation of Cant transport in ORCA05-PISCES is likely due to the underestimation of both circulation and Cant concentration. The hypothesis is supported by the analysis of the heat transported from southern latitudes at 25° N and the OVIDE section which is also underestimated by the model (Fig. 7) compared to Pérez et al (2013). Pérez et al. (2013) estimated 1.10±0.01 PW and 0.59±0.09 PW at, 25° N and OVIDE respectively, while the model yields a corresponding heat transport of 0.78±0.06 PW and 0.39±0.02 PW. The discrepancy between model and observation-based estimates of heat transport is, however, not as large as for ${}^{m}T_{Cant}^{adv}$, probably due to a better simulation of temperature than Cant concentration by the model (mean model-data bias along the section:-0.4±0.9°C for a mean value of 5°C (8% of error) for temperature, 7 µmol kg^{-1} for a mean value of 25.4 µmol kg^{-1} (27%) for Cant). The underestimation of meridional heat transport by the model reflects thus predominantly the weak MOC (Mercier et al., 2015). The comparison between biases in ${}^{m}T_{Cant}^{adv}$ and heat transport highlights the contribution of both circulation and Cant concentration in setting the discrepancy between observed and modelled meridional transport of Cant. Concerning the air-sea flux of Cant, the model estimates are larger than those derived from in situ data: Southern box: model = 0.156 ± 0.008 PgC yr^{-1}, Pérez et al. (2013) = 0.12±0.05 PgC yr^{-1}; Northern box: model = 0.044 ± 0.003 PgC yr^{-1}, Pérez et al. (2013) = 0.016±0.012 PgC yr^{-1}. The overestimation of air to sea anthropogenic CO_2 fluxes in the model could be due to the underestimation of Cant concentration in the ocean by the model, which increases the Cant gradient between the atmosphere and the ocean

and ultimately enhances the estimate of Cant uptake by the ocean. Finally, storage rates of Cant estimated for the period 2003-2011 are close to results from Pérez et al. (2013), referenced to 2004: Southern box: model = 0.216 ± 0.019, Pérez et al. (2013) = 0.280±0.011; Northern box: model = 0.045 ± 0.006 and Pérez et al. (2013) = 0.045±0.004 PgC yr^{-1}.

We derive the contribution of air-sea uptake and transport of Cant to the variability of the North Atlantic Cant inventory from the analysis of multi-annual time series of air-sea Cant fluxes, the transport divergence of Cant (defined as the difference between incoming and outgoing Cant fluxes computed at the borders of boxes) and Cant storage rate for each box. Time series were smoothed as explained previously and the potential trends were removed as noted in section II.3. Correlation coefficient (r), p-value and Coefficient of determination (r^2) are summarized in table 3. Our results suggest that, over the period 2003-2011, the rate of Cant storage between 25° N and the Nordic sills is strongly correlated with the northward transport of Cant-laden waters coming from South of 25° N (25° N: r = 0.96, p-value = 0.00; OVIDE: r = 0.95, p-value = 0.00), which explains 89% (OVIDE) to 93% (25° N) of its interannual variability. The dominance of transport over gas exchange is corroborated by observation-based assessments (Pérez et al., 2013; Zunino et al., 2014; 2015a and b).

The evaluation of model output against hydrological and biogeochemical observations, as well as the assessment of drivers of the temporal variability of Cant transport, air to sea fluxes and storage rates leads to the conclusion that major controls of the Cant budget and of its variability are well reproduced by the model for the period 2003-2011, despite the underestimation of absolute Cant concentrations and meridional circulation.

4. Long-term change in Cant fluxes and storage rate in the Subpolar North Atlantic region

In this section, we extend the analysis to the full simulation period (1958-2012) with the objective to better understand 1) the relative contribution of the variability of circulation and the increase in Cant concentration to the variability of Cant transport through the North Atlantic Ocean, and 2) the long-term change of the Cant inventory in this region as well as driving processes. For this section, the study area is limited to the mid-latitude and subpolar North Atlantic region and extends from 36° N (instead of 25° N, which includes the northern part of the subtropical region) to the Nordic sills (Mikaloff-Fletcher et al., 2003). The transport of Cant over the Nordic sills corresponds to the closure term of the regional budget.

4.1. Contribution of variability of both circulation and Cant accumulation on Cant transport variability

Figure 8 presents annual time series (1958-2012) of the magnitude of MOC and the transport of heat and Cant at 36° N and across the OVIDE section. While between 57% (OVIDE, r=0.76, p-value = 0.00) and 81% (36° N, r=0.90, p-value = 0.00) of the variance of ${}^{m}T_{HEAT}{}^{adv}$ over the study period is explained by the variability of MOCσ, it resolves only 44% of the variance of ${}^{m}T_{Cant}{}^{adv}$ at 36° N and no significant relationship is found at the OVIDE section (r=0.02, p-value = 0.90). The circulation is thus the major mechanism driving the inter-annual to decadal variability of the heat content transferred across both sections. Its impact on the variability of Cant transport is, however, masked by several other mechanisms. Figure 8 reveals that ${}^{m}T_{Cant}{}^{adv}$ is characterized by a significant and continuous increase from 0.009±0.001 PgC yr^{-1} in 1958-60 to 0.050±0.018 PgC yr^{-1} in 2010-12 at 36° N and from 0.008±0.001 PgC yr^{-1} to 0.043±0.005 PgC yr^{-1} at the OVIDE section. This large increase is neither detected on ${}^{m}T_{HEAT}{}^{adv}$ (0.0016±0.0004 PW yr^{-1} at 36° N and 0.0003±0.0002 PW yr^{-1} at OVIDE) nor on MOCσ (0.015±0.006 sv yr^{-1} at 36° N and 0.003±0.007 sv yr^{-1} at OVIDE), nor on the net volume of water transported across both sections (0.001±0.001 sv yr^{-1} at 36° N and -0.000 ±0.003 sv yr^{-1} at OVIDE). The latter (net mass transport) implies an equivalent evolution (increase or decrease) of circulation strength in the upper and the lower limb of the MOC. It follows that the increase in the northward transport of Cant (${}^{m}T_{Cant}{}^{adv}$) since 1958 is due to the increase in Cant concentration in the upper limb of the MOC as suggested by Zunino et al. (2014). In order to isolate the effect of circulation, we removed the positive trend from ${}^{m}T_{Cant}{}^{adv}$. The relationship between the detrendy ${}^{m}T_{Cant}{}^{adv}$ and the magnitude of MOC (36° N : $r^2 = 0.51$; OVIDE : $r^2 = 0.02$) does not change over the period of analysis, thus suggesting that a third mechanism, air sea Cant fluxes, has a relevant role on the variability of northward transport of Cant in the subpolar North Atlantic region.

4.2. Long-term change in Cant storage rate and driving processes

In order to assess the long-term change in Cant storage rate in the Subpolar North Atlantic and to identify underlying drivers, we focus on three well-documented periods of the last decades corresponding to NAO phases. In the model, the response of the ocean to leading mode of North Atlantic climate variability is detected from interannual anomalies of the MOC intensity at the OVIDE section (Fig.9). The anomaly of MOC intensity is a good indicator of regional circulation strength with negative anomaly for low MOC intensity, positive anomaly for high MOC intensity (Desbruyères et al., 2013). The first period is defined by negative MOCσ anomalies from 1967 to 1977 during the low NAO event of the mid-1960s (Hurrell et al., 1995). The second period is characterized by predominantly positive values between 1985 and 1997 and corresponds to the strong NAO event of the mid-1990s (Hurrell et al., 1995; Osborn, 2006). The third period is associated with low NAO once again (Osborn 2006; 2011) and a significant decrease in MOC intensity since 2002. To identify processes driving the long term change in Cant storage rate, modeled time series are smoothed with a 10 year time-window and positive trends are removed (section II.3, Fig. S3). As a consequence, time series are reduced to the period 1964-2006.

Figure 10 provides the budget of Cant for two boxes, North and South of the OVIDE section. In both regions, the significant increase in MOC intensity recorded between 1967-77 (low NAO phase; 36° N: 11.1±0.1 Sv; OVIDE: 12.5±0.2 Sv) and 1985-97 (strong NAO phase; 36° N: 11.8±0.2 Sv; OVIDE : 13.3±0.2 Sv) is concomitant to a significant increase in incoming and outgoing lateral Cant fluxes (74%), as well as in regional air-sea Cant fluxes (70%) and Cant storage rate (70% to 77%). The high (85-97) to low (2002-06) NAO transition phase is nevertheless characterized by a rather homogeneous yet not significant decrease in MOC magnitude at 36° N (11.8±0.2 Sv to 11.7±0.2 Sv) and across the OVIDE section (13.3±0.2 Sv to 12.9±0.2 Sv). South of the OVIDE section, this is concomitant to a progressive and significant intensification by 29% in northward transport of Cant at 36° N and 8% in air-sea Cant fluxes. North of the OVIDE section, the high to low NAO transition phase coincides with an average increase by 15% in incoming and outgoing Cant fluxes (transport and gas exchange), in opposition to results by Pérez et al. (2013). The large interannual variability of these fluxes revealed by Figs. 8 and S3 highlighted the significant role played by the time window size on the trend evaluation (e.g. consider trend between 1990-91 and 1999-2000 in the model at the OVIDE section) that could explain differences observed with Pérez et al. (2013). The increase in Cant fluxes for each box is, however, not as large over the 16-year period (1985-2006, from strong to low NAO) compared to 1967-1997 (from low to strong NAO) (+70-72%) and lead to an increase in regional Cant budget of 13% (south) to 19% (north). Moreover, statistical analysis of each individual NAO period shows that the regional Cant storage rate is strongly correlated with the air sea Cant fluxes during the strong NAO phase (85-97, South: $r = 0.94$, p-value = 0.00, $r^2 = 0.88$; North : $r = 0.97$, p-value = 0.00, $r^2 = 94$; table 3, hatched arrows on Fig. 10), consistent with the strong ventilation observed during this period (e.g. Sarafanov, 2009). It is nevertheless related to Cant transport divergence (incoming – outgoing Cant transport) during the low NAO phase (67-77: South: $r = 0.81$, p-value = 0.00, $r^2 = 0.66$; North : $r = 0.99$ p-value = 0.05, $r^2 = 98$; 2002-06 : South: $r = 0.96$, p-value = 0.01, $r^2 = 0.92$; North : $r = 0.93$, p-value = 0.02, $r^2 = 0.87$; table 3), consistent with result from section III. Although the transport divergence of Cant explains more than 70% of the interannual variability of the regional Cant storage rate over these two low NAO periods with low atmospheric forcing, its longer-term mean values close to zero (67-77; 85-97; 2002-06) cannot explain those of Cant inventory in the subpolar North Atlantic region (Fig. 10). Over the period 1964-2006, the Cant storage rate is in fact strongly correlated to the air to sea anthropogenic CO_2 exchange (south : r = 0.92, p-value = 0.00; north : r = 0.77, p-value = 0.00, table 3), as opposed to the transport divergence recorded in both region (1964 to 2006, south : r = -0.53, p-value = 0.00; north : r^2 = 0.34, p-value = 0.02). The long term change in air-sea Cant fluxes explains thus 59% (north) to 84% (south) of the multi decadal variability of Subpolar North Atlantic Cant inventory. As the anthropogenic CO_2 concentration increase in the atmosphere, the North Atlantic Cant inventory increase substantially.

To conclude, although the interannual variability of Cant storage rate in the Subpolar North Atlantic region is controlled by the northward advective transport divergence during the low NAO phase, its long term change is driven by air to sea anthropogenic CO_2 exchange over the period 1964-2006. Moreover, the northward advective transport of Cant, modulated by the MOC intensity, seems to be also controlled by the increasing Cant concentration in the upper limb of MOC through preconditioning in the subtropical region. Our model analysis suggests that assuming unabated emissions of CO_2, the storage rate of Cant in the Subpolar North Atlantic is expected to increase assuming MOC fluctuations within observed boundaries. However, under a future strong decrease in MOC in response to global warming (IPCC projection 25%, Collins et al., 2013) the storage rate might nevertheless decrease.

References

Álvarez, M., Pérez, F. F., Bryden, H., & Ríos, A. F. : Physical and biogeochemical transports structure in the North Atlantic subpolar gyre, J Geophys Res*: Oceans*, *109*(C3), 2004.

Aumont, O., and Bopp, L.: Globalizing results from ocean in situ iron fertilization studies, Global Biogeochem Cy, *20*(2), 2006.

Barnier, B., Madec, G., Penduff, T., Molines, J. M., Treguier, A. M., Le Sommer, J., Beckmann, A., Biastoch, A., Böning, C., Dengg, J., Derval, C., Durand, E., Gulev, S., Remy, E., Talandier, C., Theetten, S., Maltrud, M., McClean, J., and De Cuevas, B.: Impact of partial steps and momentum advection schemes in a global ocean circulation model at eddy-permitting resolution, Ocean Dynam., 56, 543–567, 2006

Bourgeois, T., Orr, J. C., Resplandy, L., Terhaar, J., Ethé, C., Gehlen, M., and Bopp, L.: Coastal-ocean uptake of anthropogenic carbon, Biogeosciences 13, 4167-4185, doi:10.5194/bg-13-4167-

2016, 2016.

Brodeau, L., Barnier, B., Treguier, A. M., Penduff, T. and Gulev, S.: An ERA40-based atmospheric forcing for global ocean circulation models, Ocean Modelling, 31(3), 88-104, 2010.

Bryden, H. L. and Imawaki, S.: Ocean heat transport, International Geophysics Series, 77, 455-474, 2001.

Bryden, H. L., Longworth, H. R. and Cunningham, S. A.: Slowing of the Atlantic meridional overturning circulation at 25 N, Nature, 438(7068), 655-657, 2005.

Ciais, P., Sabine, C., Bala, G., Bopp, L., Brovkin, V., Canadell, J., Chhabra, A., Defries, R., Galloway, J., Heimann, M., Jones, C., Le Quéré, C., Myneni, R.B., Piao, S and Thornton, P.: Carbon and other biogeochemical cycles. In: Climate Change 2013: The Physical Science Basis. Contribution of Working Group I to the Fifth Assessment Report of the Intergovernmental Panel on Climate Change [Stocker, T.F., D. Qin, G-K. Plattner, M. Tignor, S.K. Allen, J. Boschung, A. Nauels, Y. Xia, V. Bex and P.M. Midgley (eds.)]. Cambridge University Press, Cambridge, United Kingdom and New York, NY, USA, 2013.

Collins, M., Knutti, R., Arblaster, J., Dufresne, J-L., Fichefet, T., Friedlingstein, P., Gao, X., Gutwoski, W.J., Johns, T., Krinner, G., Shongwe, M., Tebaldi, C., Weaver, A.J. and Wehner, M.: Long-term Climate Change: Projections, Commitments and Irreversibility. . In: Climate Change 2013: The Physical Science Basis. Contribution of Working Group I to the Fifth Assessment Report of the Intergovernmental Panel on Climate Change [Stocker, T.F., D. Qin, G-K. Plattner, M. Tignor, S.K. Allen, J. Boschung, A. Nauels, Y. Xia, V. Bex and P.M. Midgley (eds.)]. Cambridge University Press, Cambridge, United Kingdom and New York, NY, USA, 2013.

Conkright, M. E., Locarnini, R. A., Garcia, H. E., O'Brien, T. D., Boyer, T. P., Stephens, C. and Antonov, J. I.: World Ocean Database 2001: Objective analyses, data statistics and figures, 2002

Crueger, T., Roeckner, E., Raddatz, T., Schnur, R. and Wetzel, P.: Ocean dynamics determine the response of oceanic CO_2 uptake to climate change, Clim dynam, 31(2-3), 151-168, 2008.

Curry, R. G. and McCartney, M. S.: Ocean gyre circulation changes associated with the North Atlantic Oscillation, J Phys Oceanogr, 31(12), 3374-3400, 2001.

Daniault, N., Mercier, H., Lherminier, P., Sarafanov, A., Falina, A., Zunino Rodriguez, P., Pérez, F.F., Rios, A.F., Ferron, B., Huck, T., Thierry, V. and Gladyshev, S.: The northern North Atlantic Ocean mean circulation in the early 21sr century. Prog Oceanogr, 146, 142-158. http://dx.doi.org/10.1016/j.pocean.2016.06.007, 2016.

de Boisséson, E., Thieery, V., Mercier, H., Caniaux, G and Débruyères, D. : Origin, formation and variability of the Subpolar Mode Water located over the Reykjanes Ridge. JGR (C12005), 117, doi: 10.1029/2011JC007519, 2012

Dee, D. P., Uppala, S. M., Simmons, A. J., Berrisford, P., Poli, P., Kobayaski, S., Andrae, U., Balmaseda, M. A., Balsamo, G., Bauer, P., Bechtold, P., Beljaars, A. C. M., van de Berg, L., Bidlot, J., Bormann, N., Delsol, C., Dragani, R., Fuentes, M., Geer, A. J., Haimberger, L., Healy, S. B., Hersbach, H., Hólm, E .V, Isaksen, L., Kållberg, P., Köhler, M., Matricardi, M., McNally, A. P., Monge-Sanz, B. M., Morcrette, J.-J., Park, B.-k., Peubey, C., de Rosnay, P., Tavolato, C., Thépaut, J.-N and Vitart, F.: The ERA-Interim reanalysis: configuration and perdormance of the data assimilation system, Q. J. Roy. Meteor. Soc. 137 (656), 553-597, 2011

Delworth, T. L. and Zeng, F.: The impact of the North Atlantic Oscillation on climate through its influence on the Atlantic Meridional Overturning Circulation, J Climate, 2015.

Desbruyères, D., Thierry, V. and Mercier, H: Simulated decadal variability of the meridional overturning circulation across the A25-OVIDE section, JGR 118(1), 462-475, doi: 10.1029/2012JC008342, 2013

Dickson, R., Lazier, J., Meincke, J. and Rhines, P.: Long-term coordinated changes in the convective activity of the North Atlantic. In Decadal Climate Variability (pp. 211-261). Springer Berlin Heidelberg, 1996.

García-Ibáñez, M. I, Pardo, P. C., Carracedo, L., Mercier, H., Lherminier, P., Rìos, A. F. and Pérez, F. F.: Structure, transports and transformations of the water masses in the Atlantic Subpolar Gyre, Prog. Oceanogr. 135, 18-36, http://dx.doi.org/10.1016/j.pocean.2015.03.009, 2015

Gent, P. R., and Mcwilliams, J. C.: Isopycnal mixing in ocean circulation models, J Phys Oceanogr, 20(1), 150-155, 1990.

Gruber, N., Gloor, M., Mikaloff Fletcher, S. E., Doney, S. C., Dutkiewicz, S., Follows, M. J.,Gerber, M., Jacobson, A.R., Joos, F., Lindsay, K., Menemenlis, D., Mouchet, A., Muller, S.A, Sarmiento, J.L. and Takahashi, T.:. Oceanic sources, sinks, and transport of atmospheric CO_2, Global Biogeochem Cy, 23(1), 2009.

Häkkinen, S., and Rhines, P. B.: Decline of subpolar North Atlantic circulation during the 1990s, Science, 304(5670), 555-559, 2004.

Harvey, J.: Theta-S relationships and water masses in the eastern North Atlantic, Deep Sea Res 29 (8), 1021–1033, http://dx.doi.org/10.1016/0198-0149(82)90025-5, 1982.

Hurrell, J. W.: Decadal trends in the North Atlantic Oscillation: regional temperatures and precipitation, Science, 269(5224), 676-679, 1995.

Osborn, T.J.: Recent variations in the winter North Atlantic Oscillation, Weather **61**, 353-355, 2006.

Osborn, T.J.: Winter 2009/2010 temperatures and a record-breaking North Atlantic Oscillation index, Weather **66**, 19-21, 2011.

IOC, SCOR and IAPSO: The international thermodynamic equation of seawater - 2010: Calculation and use of thermodynamic properties. Intergovernmental Oceanographic Commission, Manuals and Guides No. 56, UNESCO (English), 196 pp. Available from http://www.TEOS-10.org. See section 3.3 of this TEOS-10 Manual, 2010.

Key, R. M., Kozyr, A., Sabine, C. L., Lee, K., Wanninkhof, R., Bullister, J. L., Feely, R. A., Millero, F. J., Mordy, C. and Peng, T.-H.: A global ocean carbon climatology: Results from Global Data Analysis Project (GLODAP), Global Biogeochem Cy 18, GB4031, doi:10.1029/2004GB002247, 2004

Khatiwala, S., Tanhua, T., Fletcher, S. M., Gerber, M., Doney, S. C., Graven, H. D., Gruber, N., McKinley, G.A, Murata, A., Rıos, A.F., and Sabine, C. L.: Global ocean storage of anthropogenic carbon, Biogeosciences, 10(4), 2169-2191, 2013.

Körtzinger, A., Rhein, M., and Mintrop, L.: Anthropogenic CO2 and CFCs in the North Atlantic Ocean-A comparison of man-made tracers, Geophys Res Lett, 26(14), 2065-2068, 1999.

Lazier, J., Hendry, R., Clarke, A., Yashayaev, I. and Rhines, P.: Convection and restratification in the Labrador Sea, 1990–2000, Deep Sea Res PtI, 49(10), 1819-1835, 2002.

Le Quéré, C., Raupach, M. R., Canadell, J. G., Marland, G. and co-authors: Trends in the sources and sinks of carbon dioxide, Nature Geosciences, 2(12), 831-836, 2009.

Le Quéré, C., Peters, G. P., Andres, R. J., Andrew, R. M., and co-authors : Global carbon budget 2013, ESSD, 6, 235–263, doi:10.5194/essd-6-235-2014, 2014.

Le Quéré, C. Moriarty, R., Andrew, R.M., Peters, G.P., and co-authors: Global Carbon Budget 2014, 2015.

Lherminier, P., Mercier, H., Gourcuff, C., Alvarez, M., Bacon, S. and Kermabon, C.: Transports across the 2002 Greenland-Portugal Ovide section and comparison with 1997, J Geophys Res-Oceans, 112(C7), 2007.

Lherminier, P., Mercier, H., Huck, T., Gourcuff, C., Perez, F. F., Morin, P., Sarafanov, A., andFalina, A.: The Atlantic Meridional Overturning Circulation and the subpolar gyre observed at the A25-OVIDE section in June 2002 and 2004, Deep Sea Res Pt I 57(11), 1374-1391, 2010.

Madec, G., and Imbard, M.: A global ocean mesh to overcome the North Pole singularity, Climate Dy 12(6), 381-388, 1996.

Madec, G.: NEMO Ocean Engine, vol. 27, pp. 1–217, Note du Pole de modélisation de l'Institut Pierre-Simon Laplace, France, 2008

Marsh, R., De Cuevas, B. A., Coward, A. C., Bryden, H. L., and Álvarez, M.: Thermohaline circulation at three key sections in the North Atlantic over 1985–2002, Geophys Res Lett 32(10), 2005

McKinley, G.A., Pilcher, D.J., Fay, A.R., Lindsay, K., Long, M.C. and Lovenduski, N.S.:

Timescales for detection of trends in the ocean carbon sink. Nature, 530, 469-472, 2013.

Mercier, H., Lherminier, P., Sarafanov, A., Gaillard, F., Daniault, N., Desbruyères, D., Falina, A., Ferron, B., Gourcuff, C., Huck, T. and Thierry, V.: Variability of the meridional overturning circulation at the Greenland–Portugal OVIDE section from 1993 to 2010, Prog Oceanogr 132 (2015) 250–261, doi:10.1016/j.pocean.2013.11.001, 2015

Mikaloff Fletcher, S. E., Gruber, N., and Jacobson, A. R.: Ocean Inversion Project How-to Document Version 1.0, 18 pp. Institute for Geophysics and Planetary Physics, University of California, Los Angles, 2003

Mikaloff Fletcher, S. E., Gruber, N., Jacobson, A. R., Doney, S. C., Dutkiewicz, S., Gerber, M., Follows, M., Joos, F., Lindsay, K., Menemenlis, D., Mouchet, A., Müller, S.A. and Sarmiento, J.L.: Inverse estimates of anthropogenic CO_2 uptake, transport, and storage by the ocean. Global Biogeochem Cy 20(2), doi:10.1029/2005GB002530, 2006.

Pérez, F. F., Vazquez-Rodriguez, M., Louarn, E., Padín, X. A., Mercier, H., and Ríos, A. F. : Temporal variability of the anthropogenic CO2 storage in the Irminger Sea, Biogeosciences, 5(6), 1669-1679, 2008

Pérez, F. F., Vázquez Rodríguez, M., Mercier, H., Velo, A., Lherminier, P. and Ríos, A. F. : Trends of anthropogenic CO_2 storage in North Atlantic water masses, Biogeosciences, 7, 1789–1807, doi:10.5194/bg-7-1789-2010, 2010.

Pérez, F. F., Mercier, H., Vázquez-Rodríguez, M., Lherminier, P., Velo, A., Pardo, P. C., Roson, G., and Ríos, A. F. : Atlantic Ocean CO_2 uptake reduced by weakening of the meridional overturning circulation, Nature Geoscience, 6(2), 146-152, doi: 10.1038/NGEO1680, 2013

Pickart, R. S., Straneo, F. and Moore, G. W. K.: Is Labrador sea water formed in the Irminger basin?, Deep Sea Res Pt I 50(1), 23-52, 2003.

Pickart, R. S., Torres, D. J. and Fratantoni, P. S.: The East Greenland Spill Jet. J Phys Oceanogr 35(6), 1037-1053, 2005.

Pollard, R.T., Grifftths, M.J., Cunningham, S.A., Read, J.F., Perez, F.F. and Rios, A.F.: Vivaldi 1991 – a study of the formation, circulation and ventilation of Eastern North Atlantic Central Water, Prog Oceanogr 37, 167–192. http://dx.doi.org/10.1016/S0079-6611(96)00008-0, 1996.

Rhein, M., Fischer, J., Smethie, W. M., Smythe-Wright, D., Weiss, R. F., Mertens, C., Min, D.H., Fleischmann, U., and Putzka, A.: Labrador Sea Water: Pathways, CFC inventory, and formation rates, J Phys Oceanogr 32(2), 648-665, 2002.

Rhein, M., Kieke, D., Hüttl-Kabus, S., Roessler, A., Mertens, C., Meissner, R., Klein, B., Böning, C.W. and Yashayaev, I.: Deep water formation, the subpolar gyre, and the meridional overturning circulation in the subpolar North Atlantic, Deep-Sea Res Pt II 58(17), 1819-1832, 2011.

Sabine, C. L., Feely, R. A., Gruber, N., Key, R. M., Lee, K., Bullister, J. L., Wanninkhof, R., Wong, C.S., Wallace, D.W.R., Tilbrook, B., Millero, F.J., Peng, T-H., Kozyr, A., Ono, T. and Rios, A.F.: The oceanic sink for anthropogenic CO_2. Science 305(5682), 367-371, 2004.

Sarafanov, A.: On the effect of the North Atlantic Oscillation on temperature and salinity of the subpolar North Atlantic intermediate and deep waters. ICES Journal of Marine Science: Journal du Conseil, 66(7), 1448-1454, 2009.

Séférian, R., Ribes, A. and Bopp, L.: Detecting the anthropogenic influences on recent changes in ocean carbon uptake: Geophys. Res. Lett, 41, 5968-5977, 2014

Steinfeldt, R., Rhein, M., Bullister, J. L. and Tanhua, T.: Inventory changes in anthropogenic carbon from 1997–2003 in the Atlantic Ocean between 20 S and 65 N, Global Biogeochem Cy 23(3), 2009.

Tanhua, T., Olsson, K. A. and Jeansson, E.: Formation of Denmark Strait overflow water and its hydro-chemical composition, J Mar Sys 57(3), 264-288, 2005.

Timmermann, R., Goosse, H., Madec, G., Fichefet, T., Ethe, C. and Duliere, V.: On the representation of high latitude processes in the ORCA-LIM global coupled sea ice–ocean model. Ocean Modelling, 8(1), 175-201, 2005.

Treguier, A-M., Gourcuff, C., Lherminier, P., Mercier, H., Barnier, B., Madec, G., Molines, J-M., Penduff, T., Czeschel, L., Böning, C.W.: Internal and Forced variability along a section between Greenland and Portugal in the CLIPPER Atlantic model. Ocean Dynam 56 (5-6), 568-580, doi:10.1007/s10236-006-0069-y, 2006

Tsuchiya, M., Talley, L.D., McCartney, M.S.: An eastern Atlantic section from Iceland southward across the equator. Deep Sea Res Pt A 39 (11), 1885–1917. http://dx.doi.org/10.1016/0198-0149(92)90004-D, 1992

Våge, K., Pickart, R. S., Sarafanov, A., Knutsen, Ø., Mercier, H., Lherminier, P., van Aken, H.M., Meincke, J., Quadfasel, D. and Bacon, S.: The Irminger Gyre: Circulation, convection, and interannual variability, Deep-Sea Res Pt I 58(5), 590-614, doi:10.1016/j.dsr.2011.03.001, 2011.

van Aken, H.M. and Becker, G.: Hydrography and through-flow in the northeastern North Atlantic Ocean: the NANSEN project, Prog Oceanogr 38 (4), 297–346, http://dx.doi.org/10.1016/S0079-6611(97)00005-0., 1996

van Aken, H. M. : The hydrography of the mid-latitude northeast Atlantic Ocean: I: The deep water masses, Deep-Sea ResPt I 47(5), 757-788, 2000.

Vázquez-Rodríguez, M., Padin, X. A., Ríos, A. F., Bellerby, R. G. J. and Pérez, F. F.: An upgraded carbon-based method to estimate the anthropogenic fraction of dissolved CO_2 in the Atlantic

Ocean, Biogeosciences Discuss., 6, 4527–4571, doi:10.5194/bgd-6-4527-2009, 2009.

Velo, A., Pérez, F. F., Lin, X., Key, R. M., Tanhua, T., de la Paz, M., Olsen, A., van Heuven, S., Jutterström, S. and Ríos, A. F.: CARINA data synthesis project: pH data scale unification and cruise adjustments, Earth Syst. Sci. Data, 2, 133–155, doi:10.5194/essd-2-133-2010, 2010.

Wanninkhof, R.: Relationship between wind speed and gas exchange over the ocean, Jeophys Res 97(C5), 7373-7382, 1992.

Wanninkhof, R., Park, G.H., Takahashi, T., Sweeney, C., Feely, R.A., Nojiri, Y., Gruber, N., Doney, S.C., McKinley, G.A., Lenton, A., Le Quere, C., Heinze, C. Schwinger, J., Graven, H., and Khatiwala, S.: Global Ocean carbon uptake: Magnitude, variability and trend, Biogeosciences 10, 1983-2000, doi:10.5194/bg-10-1983-2013, 2013

Yashayaev, I.: Hydrographic changes in the Labrador Sea, 1960–2005, Prog Oceanogr 73(3), 242-276, 2007.

Yashayaev, I. and Dickson, B.: Transformation and fate of overflows in the northern North Atlantic. In Arctic–Subarctic Ocean Fluxes (pp. 505-526). Springer Netherlands, 2008.

Zunino, P., Garcia-Ibanez, M. I., Lherminier, P., Mercier, H., Ríos, A. F. and Pérez, F. F.: Variability of the transport of anthropogenic CO2 at the Greenland-Portugal OVIDE section: Controlling mechanisms, Biogeosciences, 11, 2375–2389, doi:10.5194/bg-11-2375-2014, 2014

Zunino, P., Lherminier, P., Mercier, H., Padín, X. A., Ríos, A. F. and Pérez, F. F.: Dissolved inorganic carbon budgets in the eastern subpolar North Atlantic in the 2000s from in situ data, Geophys Res Lett 42(22), 9853-9861, 2015.

Zunino, P., Pérez, F. F., Fajar, N. M., Guallart, E. F., Ríos, A. F., Pelegrí, J. L. and Hernández-Guerra, A.: Transports and budgets of anthropogenic CO_2 in the tropical North Atlantic in 1992–1993 and 2010–2011, Global Biogeochem Cy, 29(7), 1075-1091, 2015.

Acknowledgment

For this work, VR was funded through the EU FP7 project CARBOCHANGE (grant 264879). Simulations were made using HPC resources from GENCI-IDRIS (grant x2015010040). We are grateful to Christian Ethe, who largely contributed to obtain Cant transport in online over the period 2003-2011. We want to acknowledge HM (supported by CNRS and the ATLANTOS H2020 project (GA 633211)) and colleagues for leading OVIDE project (supported by French research institutions, IFREMER and CNRS/INSU).

Table captures

Table 1: OVIDE cruises

OVIDE name	Month/year	Vessel	Reference	CARINA expocode
OVIDE 2002	06-07/2002	N/O Thalassa	Lherminier et al., 2007	35TH20020611
OVIDE 2004	06-07/2004	N/O Thalassa	Lherminier et al., 2010	35TH20040604
OVIDE 2006	05-06/2006	R/V Maria S. Merian	Gourcuff et al., 2011	06MM20060523
OVIDE 2008	06-07/2008	N/O Thalassa	Mercier et al. 2015	35TH20080610
OVIDE 2010	06-07/2010	N/O Thalassa	Mercier et al., 2015	35TH20100608

Table 2: Model-data comparison over the period covered by OVIDE cruises (2002-2010). Average and standard deviation (SD) for observation-based estimates (column 2) and model output (columns 3 to 5). Model output: (1) June average with SD being a measure of interannual variability, (2) average year with SD corresponding to the average seasonal variability, or (3) average over the full period with SD being representative of total variability (interannual + seasonnal).

	OVIDE data set	**ORCA05-PISCES**		
		June only	**average year**	**full period**
Mass transport (sv)	0.74±0.75	0.19±0.33	0.67±0.24	0.67±0.46
MOCσ (sv)	15.5±2.3	13.4±0.6	12.7±0.6	13.4±2.43
σMOC (kg m^{-3})	32.14	32.02±0.05	31.95±0.04	31.98±0.12
$[\mathrm{Cant}]_{\mathrm{section}}$ (µmol kg^{-1})	25.4±1.8	18.4±1.1	18.4±1.1	18.4±1.1
$[\mathrm{Cant}]_{\mathrm{upper}}$ (µmol kg^{-1})	45.2±3.0	38.9±3.0	39.4±3.0	39.4±3.0
$[\mathrm{Cant}]_{\mathrm{lower}}$ (µmol kg^{-1})	19.4±1.6	14.8±1.0	14.9±1.0	14.9±1.0
$\Delta[\mathrm{Cant}^{\mathrm{up\text{-}low}}]$ (µmol kg^{-1})	25.8±1.4	24.1±1.6	24.6±1.6	24.5±2.2

Table 3: Correlation coefficient (r), p-value and coefficient of determination (r^2) between the time rate of change (Trate), the divergence of Cant transport (DTcant) and air sea Cant fluxes (Fcant) for the three boxes. DTcant = incoming – outgoing Cant fluxes across the boundaries of boxes.

Box 25° N to OVIDE section	
2003-11	Trate/DTcant : r = 0.96, p-value = 0.00, r^2 = 0.93 Trate/Fcant : r = - 0.54, p-value = 0.00, r^2 = 0.30
Box OVIDE section to Nordic sills	
2003-11	Trate/DTcant : r = 0.95, p-value = 0.00, r^2 = 0.89 Trate/Fcant : r = - 0.71, p-value = 0.00, r^2 = 0.51
Box 36° N to OVIDE section	
1967-77	Trate/DTcant : r = 0.81, p-value = 0.00, r^2 = 0.66 Trate/Fcant : r = - 0.66, p-value = 0.02, r^2 = 0.45
1985-97	Trate/DTcant : r = -0.65, p-value = 0.02, r^2 = 0.42 Trate/Fcant : r = 0.94, p-value = 0.00, r^2 = 0.88
2002-06	Trate/DTcant : r = 0.96, p-value = 0.01, r^2 = 0.92 Trate/Fcant : r = 0.61, p-value = 0.27, r^2 = 0.37
1964-06	Trate/DTcant : r = -0.53, p-value = 0.00, r^2 = 0.28 Trate/Fcant : r = 0.92, p-value = 0.00, r^2 = 0.84

Box OVIDE section to Nordic sills	
1967-77	Trate/DTcant : r = 0.99, p-value = 0.05, r^2 = 0.98
	Trate/Fcant : r = - 0.22, p-value = 0.05, r^2 = 0.05
1985-97	Trate/DTcant : r = 0.87, p-value = 0.00, r^2 = 0.74
	Trate/Fcant : r = 0.97, p-value = 0.00, r^2 = 0.94
2002-06	Trate/DTcant : r = 0.93, p-value = 0.02, r^2 = 0.87
	Trate/Fcant : r = 0.60, p-value = 0.28, r^2 = 0.36
1964-06	Trate/Dtcant : r = 0.34, p-value = 0.02, r^2 = 0.12
	Trate/Fcant : r = 0.77, p-value = 0.00, r^2 = 0.59

Figures captions

Fig. 1: Year 2010 column inventory (molC m^{-2}) of anthropogenic Carbon: (a) model output and (b) after Khatiwala et al. [2009].

Fig. 2: Year 2010 North Atlantic column inventory (molC m^{-2}) of anthropogenic Carbon: model output from 25° N to Greenland-Iceland-Scotland sills. The OVIDE cruise track between Greenland and Portugal is indicated by the continuous line.

Fig. 3: Water column distribution of (a-b) salinity, (c-d) dissolved oxygen (µmol kg^{-1}) and (e-f) dissolved silica (µmol kg^{-1}) along the Greenland-Portugal OVIDE section in June 2002: model output (left) and sampled during the OVIDE cruise (right). Water masses and currents cited in section III.1 are identified on the right panel: East North Atlantic Central Water (ENACW), Mediterranean Water (MW), Labrador Sea Water (LSW), lower North-East Atlantic Deep Water (NEADWl) and Eastern Reykjanes Ridge Current (ERRC). Four basins are delimited by grey dashed vertical lines. From Greenland to the coast of Portugal: Irminger basin (IrB), Iceland basin (IcB), East – North Atlantic basin (ENAB) and Iberian Basin (IbB).

Fig. 4. Monthly evolution of the net volume transported across the Greenland-Portugal OVIDE section (Sv): model output (black continuous lines) and estimates derived from the OVIDE data set (orange dots) over the period 2002-2010

Fig. 5. Vertically integrated cumulative mass transport (Sv): model output for the month of June over the period 2002-10 (continuous line for mean value; shadows for confidence interval) (a) from bottom to each specific density level (σ_1 with 0.01 kg m^{-3} resolution), note that the sign of the profile has been changed, and (b) from Greenland to Portugal (km) compared to estimates derived

from OVIDE (dashed lines). On panel (a) the black horizontal lines indicate the density of MOCσ maximum corresponding to the separation between the upper (red) and lower (blue) limbs of MOC, in the model (σ_{MOC} = 32.02±0.05 kg m^{-3}, black continuous line) and observation-based assessments (σ_{MOC} = 32.14 kg m^{-3}, Zunino et al., 2014; black dashed line). On panel (b) the position of the Western and Eastern NAC branches as well as the Irminger current, a NAC modified branch, are indicated in grey (Mercier et al., 2015).

Fig. 6 : Water column distribution of anthropogenic C concentrations (µmol kg^{-1}) along the Greenland-Portugal OVIDE section in June 2002: (a) model output and (b) as estimated from the OVIDE data set. The difference between these both assessments (model – OVIDE) over the OVIDE period (June 2002-04-06-08-10) and its standard deviation are displayed on Fig. c and d. Grey dashed lines delimit the four basins identified on Fig. 3. Black continuous and dashed lines indicate the limit between the upper and the lower limbs of the MOC in the model and the OVIDE data set.

Fig. 7: Anthropogenic C budget of the Subtropical and Subpolar North Atlantic regions over the period 2003-2011. Average values and their standard deviation were estimated from smoothed time series. The horizontal arrows show the lateral Cant transport in PgC yr^{-1} (black font). Red numbers in the panel indicate the Cant storage rate in PgC yr^{-1}. The vertical arrows show the anthropogenic air-sea CO_2 fluxes in PgC yr^{-1}. Green numbers represent the heat transport across sections in PW. Boundaries and surface area (m^2) of each box are indicated below the panels.

Fig. 8: Simulated annual time series of MOC magnitude (MOCσ, Sv) and transport of heat (PW) and anthropogenic C (PgC yr^{-1}) at 36° N and at the OVIDE section estimated over the period 1958-2012.

Fig. 9: Simulated annual time series of MOCσ anomaly over the period 1958-2012 along the Greenland-Portugal OVIDE section. Three particular periods are highlighted by grey areas: 1967-77 characterized by a weak MOCσ (negative MOCσ anomaly), 1985-97 with a strong MOCσ (positive MOCσ anomaly) and since 2002 (negative trend in MOCσ).

Fig. 10: Anthropogenic C budget for the period 1967-1977 (weak MOCσ), 1985-1997 (strong MOCσ) and 2002-2006 (MOCσ negative trend) in the Subpolar North Atlantic region defined from 36° N to Nordic sill and divided in two boxes by the OVIDE section. Average values and their standard deviation were estimated from smoothed times series (Fig. S3). Vertical arrows show the

air to sea anthropogenic CO_2 fluxes in PgC yr^{-1}, black horizontal arrows correspond to the advective transport of Cant across section in PgC yr^{-1}. Red numbers indicate the Cant storage rate in each box. The size of arrows and fonts used for the storage rate are proportional to the 2002-2006 budget. Hatched arrows indicate a strong correlation between the term and the regional Cant storage rate over the period of interest.

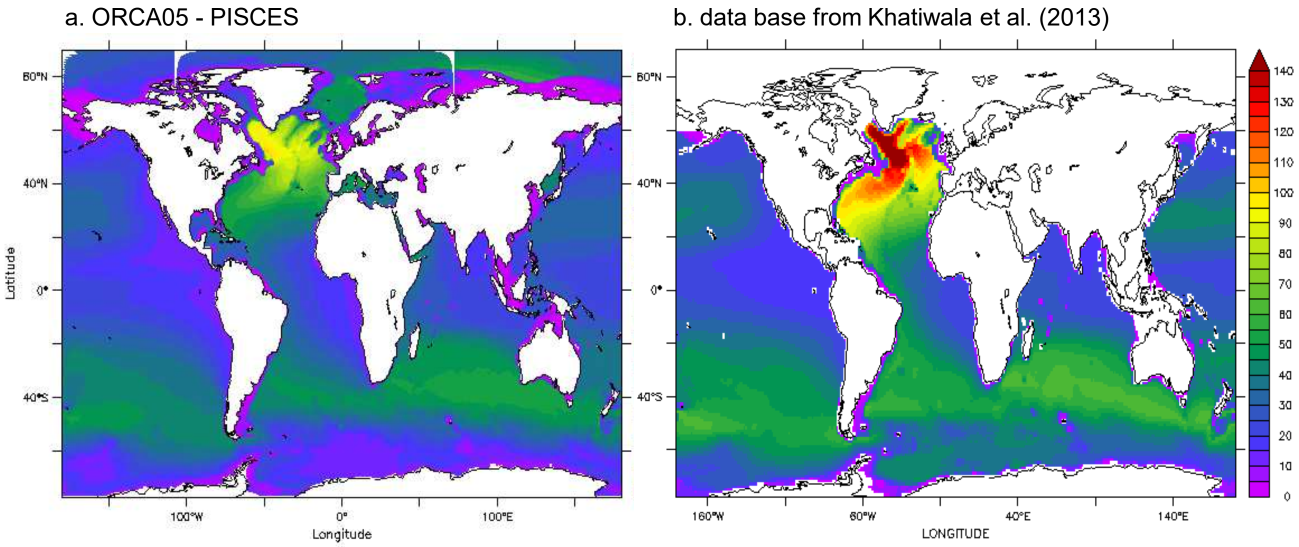
a. ORCA05 - PISCES

b. data base from Khatiwala et al. (2013)

Fig. 1: Year 2010 column inventory (molC m^{-2}) of anthropogenic Carbon: (a) model output and (b) after Khatiwala et al. [2009].

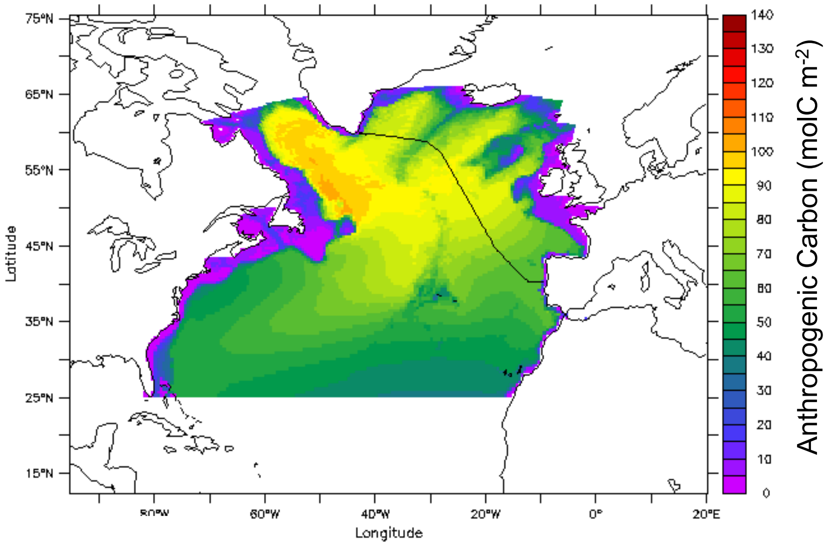

Fig. 2: Year 2010 North Atlantic column inventory (molC m^{-2}) of anthropogenic Carbon: model output from 25° N to Greenland-Iceland-Scotland sills. The OVIDE cruise track between Greenland and Portugal is indicated by the continuous line.

Biogeosciences Discuss., doi:10.5194/bg-2016-541, 2017
Manuscript under review for journal Biogeosciences
Published: 4 January 2017

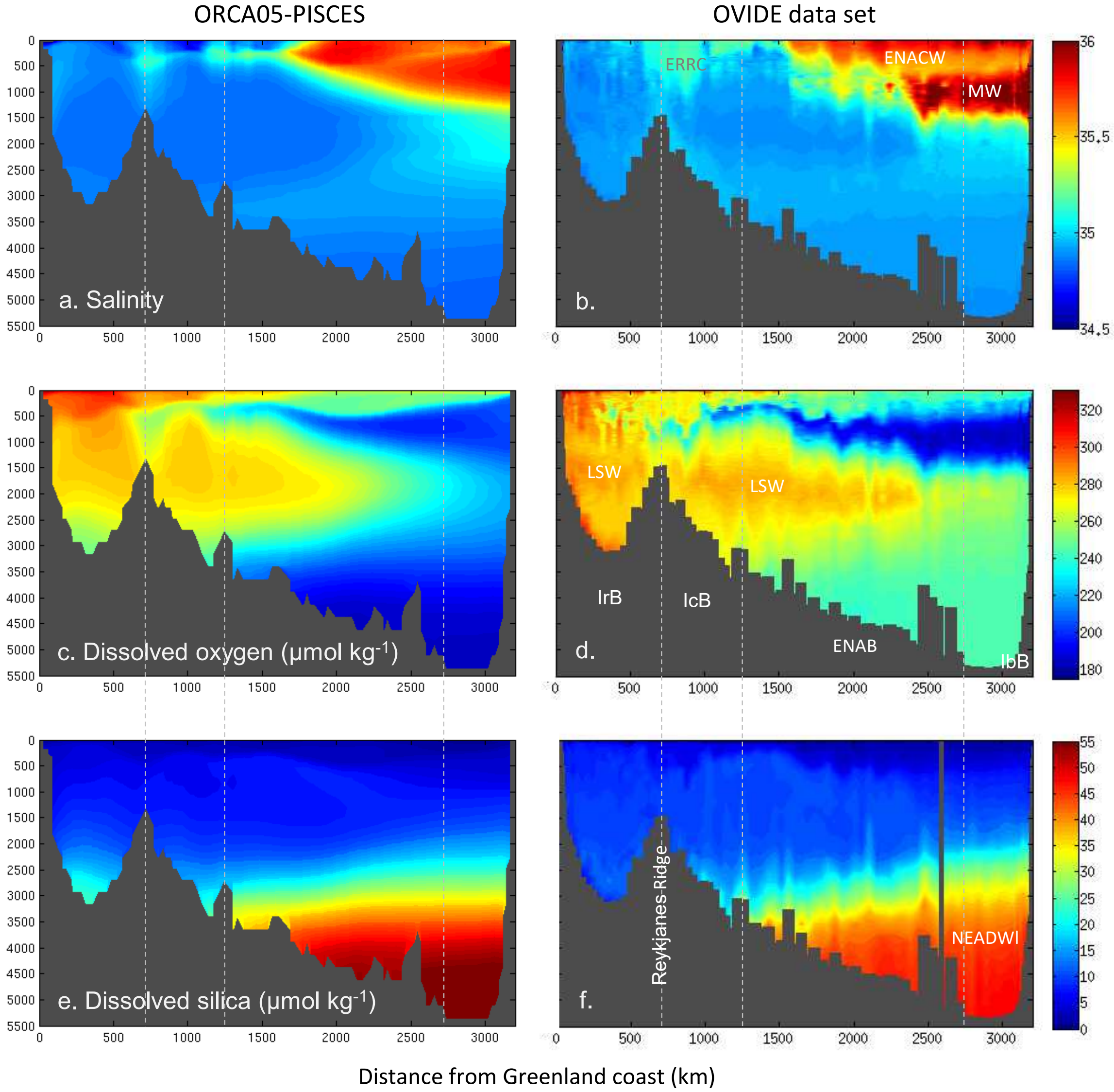

Fig. 3: Water column distribution of (a-b) salinity, (c-d) dissolved oxygen (µmol kg^{-1}) and (e-f) dissolved silica (µmol kg^{-1}) along the Greenland-Portugal OVIDE section in June 2002: model output (left) and sampled during the OVIDE cruise (right). Water masses and currents cited in section III.1 are identified on the right panel: East North Atlantic Central Water (ENACW), Mediterranean Water (MW), Labrador Sea Water (LSW), lower North-East Atlantic Deep Water (NEADWl) and Eastern Reykjanes Ridge Current (ERRC). Four basins are delimited by grey dashed vertical lines. From Greenland to the coast of Portugal: Irminger basin (IrB), Iceland basin (IcB), East – North Atlantic basin (ENAB) and Iberian Basin (IbB).

Biogeosciences Discuss., doi:10.5194/bg-2016-541, 2017
Manuscript under review for journal Biogeosciences
Published: 4 January 2017

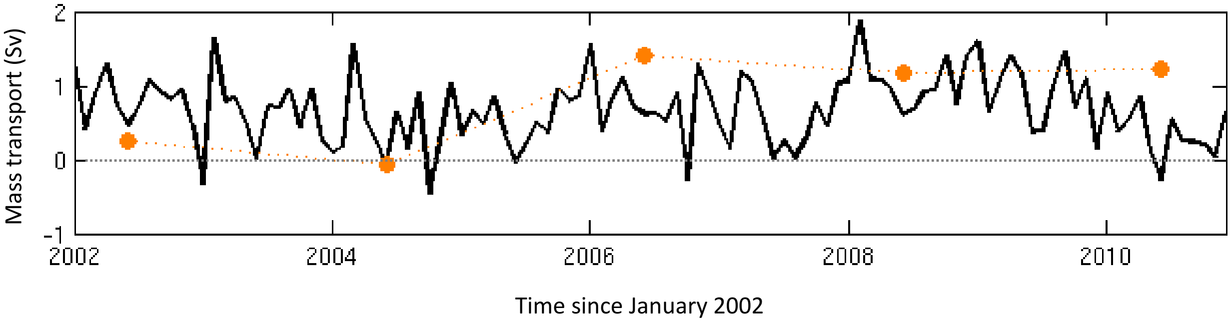

Fig. 4. Monthly evolution of the net volume transported across the Greenland-Portugal OVIDE section (Sv): model output (black continuous lines) and estimates derived from the OVIDE data set (orange dots) over the period 2002-2010

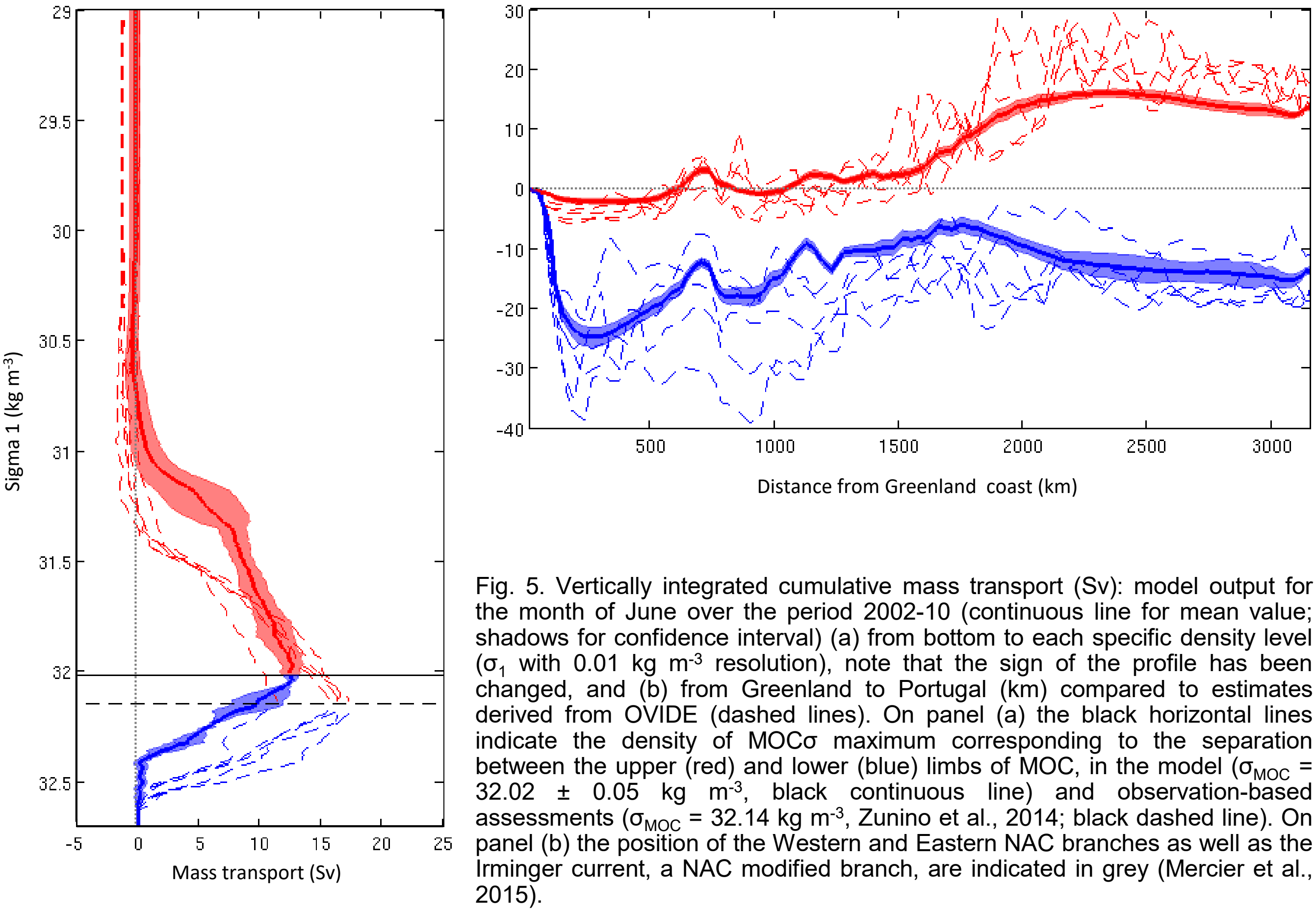

Fig. 5. Vertically integrated cumulative mass transport (Sv): model output for the month of June over the period 2002-10 (continuous line for mean value; shadows for confidence interval) (a) from bottom to each specific density level (σ_1 with 0.01 kg m^{-3} resolution), note that the sign of the profile has been changed, and (b) from Greenland to Portugal (km) compared to estimates derived from OVIDE (dashed lines). On panel (a) the black horizontal lines indicate the density of MOCσ maximum corresponding to the separation between the upper (red) and lower (blue) limbs of MOC, in the model (σ_{MOC} = 32.02 ± 0.05 kg m^{-3}, black continuous line) and observation-based assessments (σ_{MOC} = 32.14 kg m^{-3}, Zunino et al., 2014; black dashed line). On panel (b) the position of the Western and Eastern NAC branches as well as the Irminger current, a NAC modified branch, are indicated in grey (Mercier et al., 2015).

Biogeosciences Discuss., doi:10.5194/bg-2016-541, 2017
Manuscript under review for journal Biogeosciences
Published: 4 January 2017

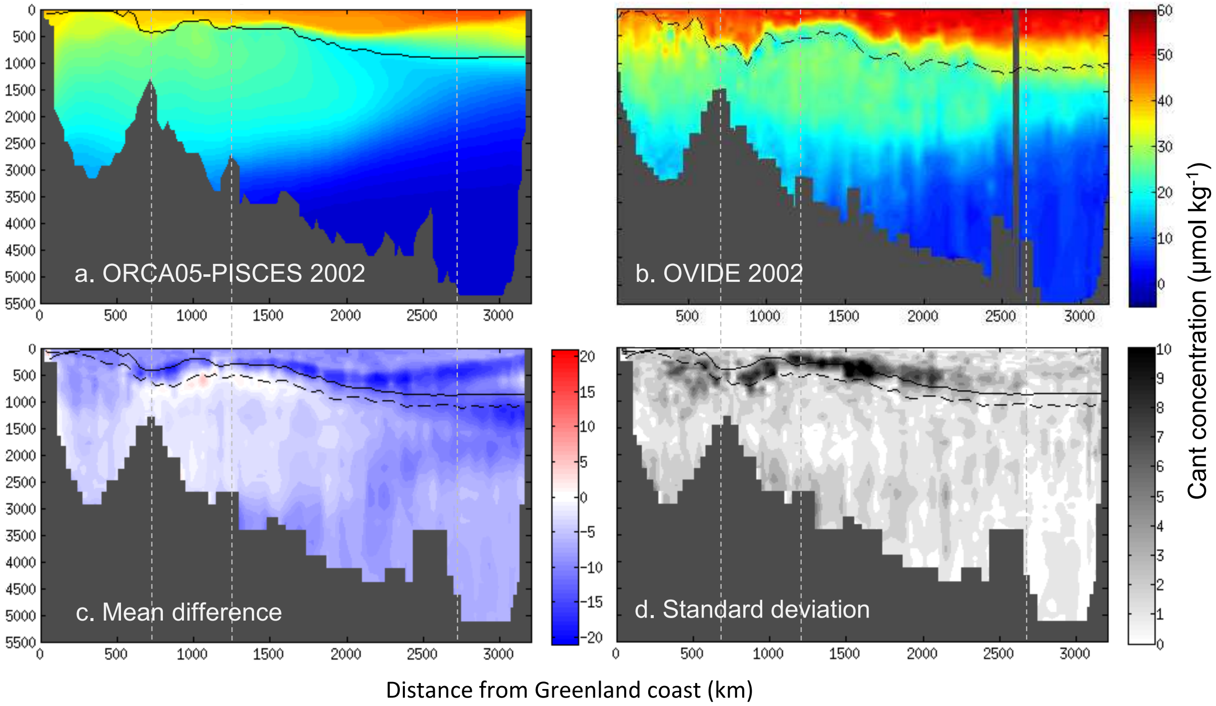

Fig. 6 : Water column distribution of anthropogenic C concentrations (µmol kg^{-1}) along the Greenland-Portugal OVIDE section in June 2002: (a) model output and (b) as estimated from the OVIDE data set. The difference between these both assessments (model – OVIDE) over the OVIDE period (June 2002-04-06-08-10) and its standard deviation are displayed on figures (c) and (d). Grey dashed lines delimit the four basins identified on figure 3. Black continuous and dashed lines indicate the limit between the upper and the lower limbs of the MOC in the model and the OVIDE data set.

Biogeosciences Discuss., doi:10.5194/bg-2016-541, 2017
Manuscript under review for journal Biogeosciences
Published: 4 January 2017

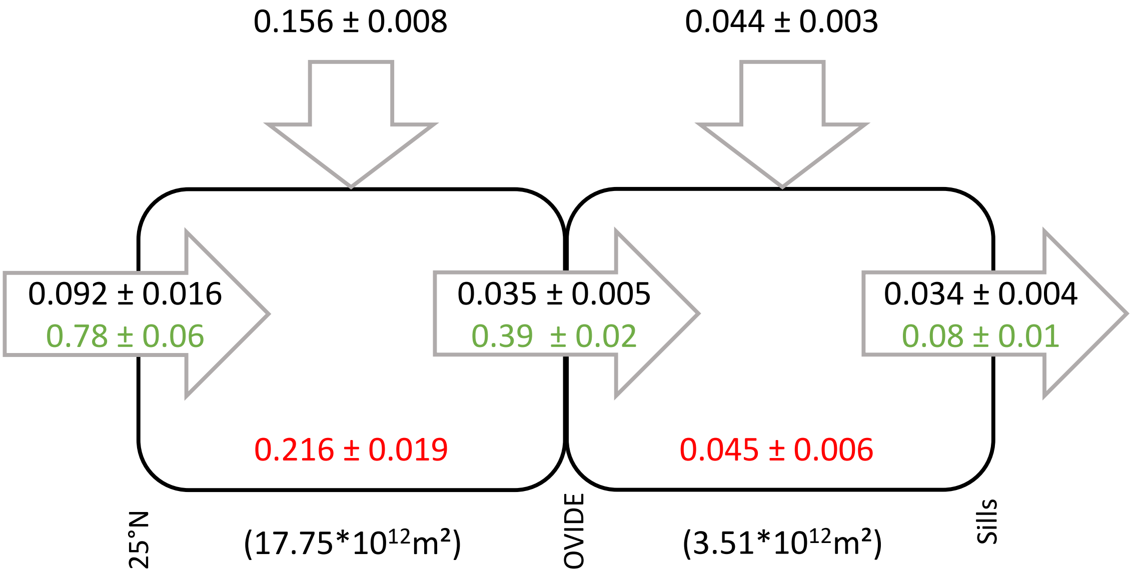

Fig. 7: Anthropogenic C budget of the Subtropical and Subpolar North Atlantic regions over the period 2003-2011. Average values and their standard deviation were estimated from smoothed time series. The horizontal arrows show the lateral Cant transport in PgC yr^{-1} (black font). Red numbers in the panel indicate the Cant storage rate in PgC yr^{-1}. The vertical arrows show the anthropogenic air-sea CO_2 fluxes in PgC yr^{-1}. Green numbers represent the heat transport across sections in PW. Boundaries and surface area (m²) of each box are indicated below the panels.

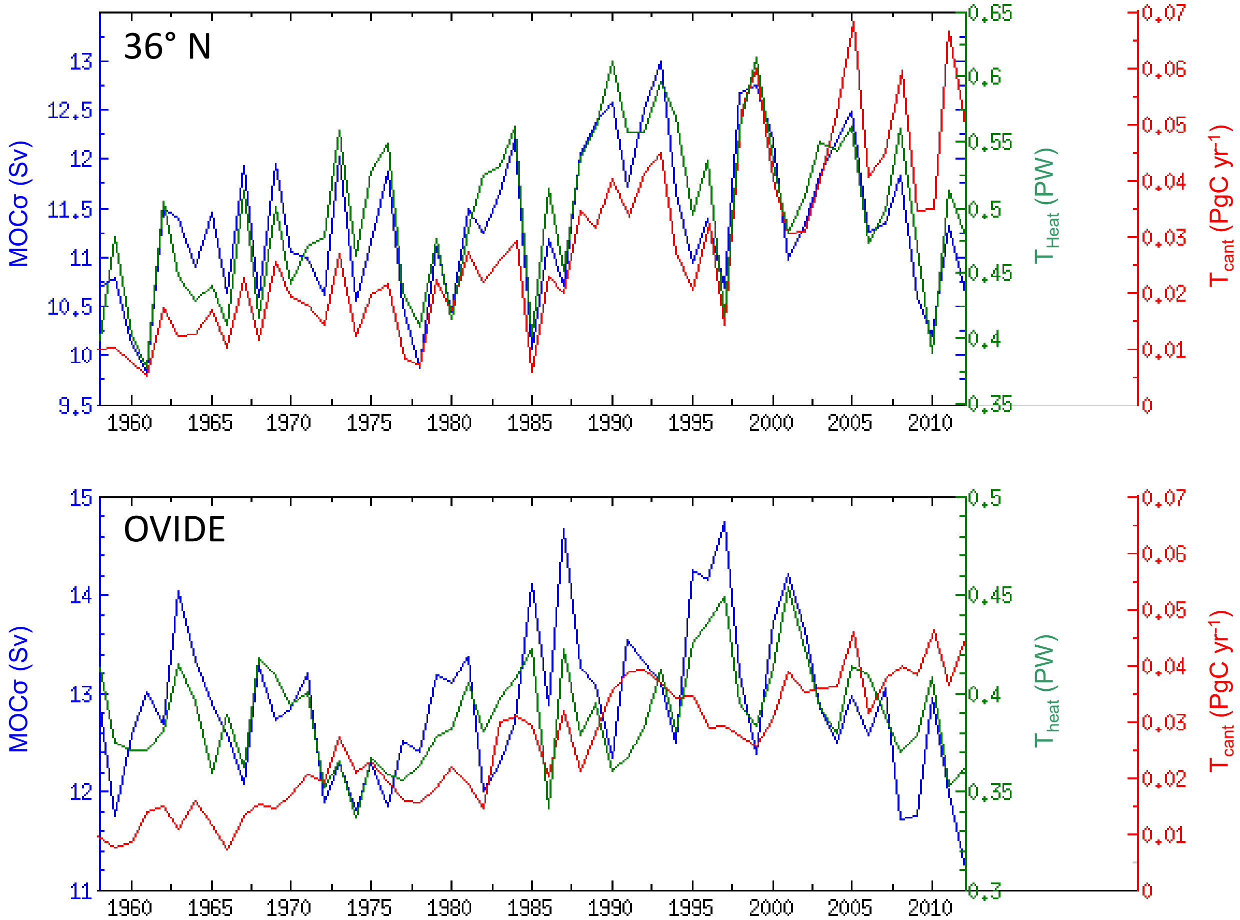

Fig. 8: Simulated annual time series of MOC magnitude (MOCσ, Sv) and transport of heat (PW) and anthropogenic C (PgC yr^{-1}) at 36° N and at the OVIDE section estimated over the period 1958-2012.

Biogeosciences Discuss., doi:10.5194/bg-2016-541, 2017
Manuscript under review for journal Biogeosciences
Published: 4 January 2017

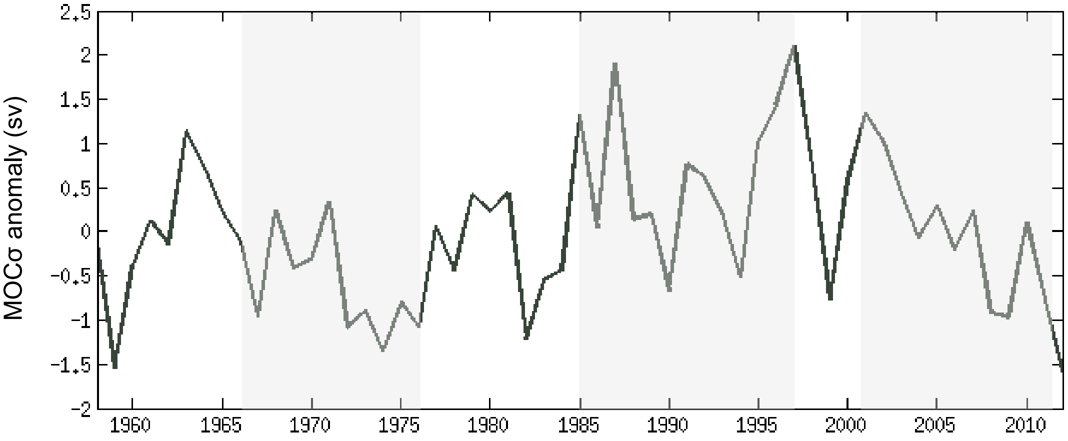

Fig. 9: Simulated annual time series of MOCσ anomaly over the period 1958-2012 along the Greenland-Portugal OVIDE section. Three particular periods are highlighted by grey areas: 1967-77 characterized by a weak MOCσ (negative MOCσ anomaly), 1985-97 with a strong MOCσ (positive MOCσ anomaly) and since 2002 (negative trend in MOCσ).

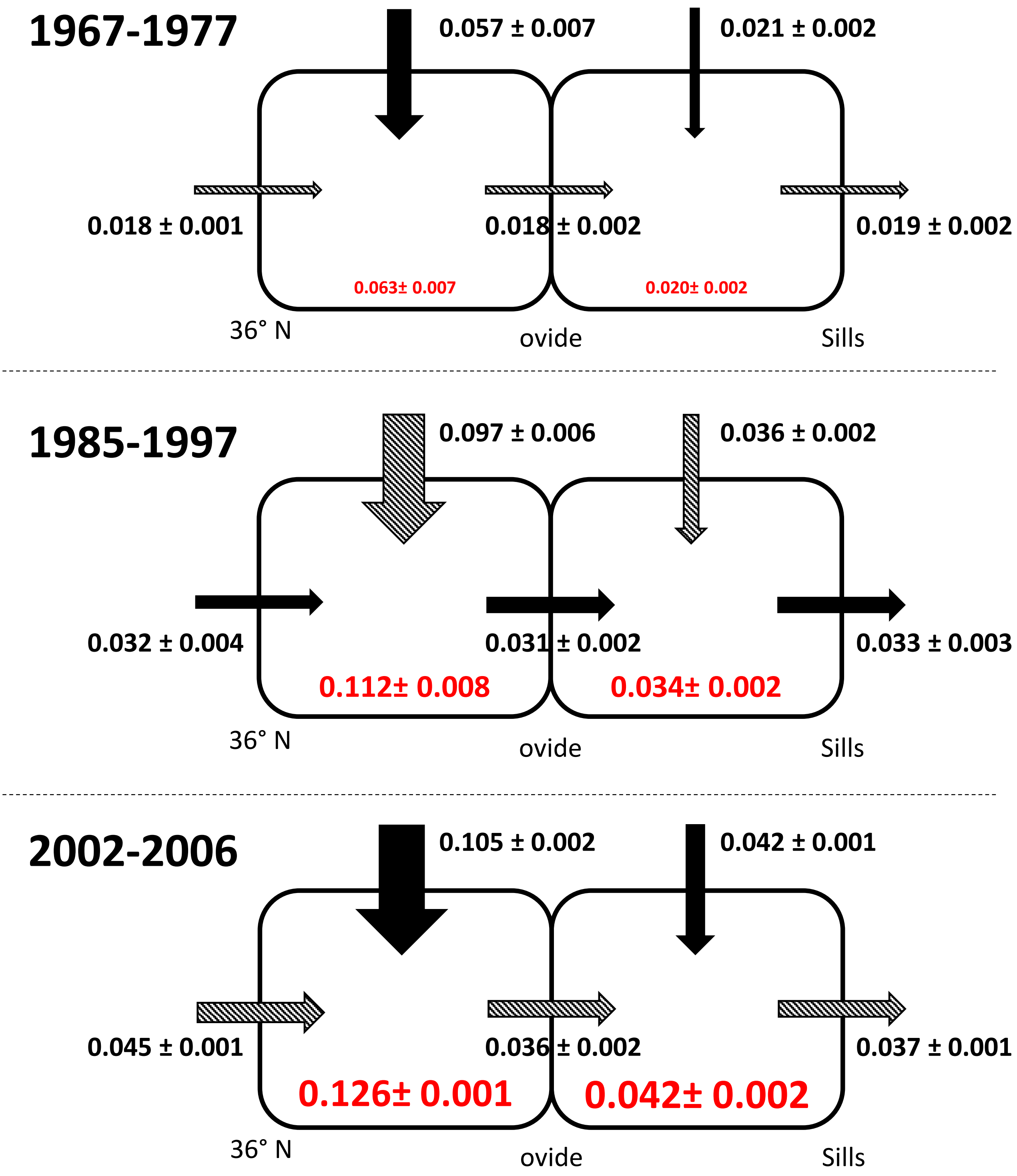
1967-1977
0.057 ± 0.007
0.021 ± 0.002
0.018 ± 0.001
0.018 ± 0.002
0.019 ± 0.002
0.063± 0.007
0.020± 0.002
36° N
ovide
Sills
1985-1997
0.097 ± 0.006
0.036 ± 0.002
0.032 ± 0.004
0.031 ± 0.002
0.033 ± 0.003
0.112± 0.008
0.034± 0.002
36° N
ovide
Sills
2002-2006
0.105 ± 0.002
0.042 ± 0.001
0.045 ± 0.001
0.036 ± 0.002
0.037 ± 0.001
0.126± 0.001
0.042± 0.002
36° N
ovide
Sills

Biogeosciences Discuss., doi:10.5194/bg-2016-541, 2017
Manuscript under review for journal Biogeosciences
Published: 4 January 2017

Fig. 10: Anthropogenic C budget for the period 1967-1977 (weak MOCσ), 1985-1997 (strong MOCσ) and 2002-2006 (MOCσ negative trend) in the Subpolar North Atlantic region defined from 36° N to Nordic sill and divided in two boxes by the OVIDE section. Average values and their standard deviation were estimated from smoothed times series (Fig. S3). Vertical arrows show the air to sea anthropogenic CO_2 fluxes in PgC yr^{-1}, black horizontal arrows correspond to the advective transport of Cant across section in PgC yr^{-1}. Red numbers indicate the Cant storage rate in each box. The size of arrows and fonts used for the storage rate are proportional to the 2002-2006 budget. Hatched arrows indicate a strong correlation between the term and the regional Cant storage rate over the period of interest.